CIPS PMC Level 2 Data: Orbit-by-Orbit Cloud Parameters

Last Updated August 2020

1. Introduction

Version 5.20 CIPS polar mesospheric cloud (PMC) Level 2 data files consist of measurements of cloud parameters on an orbit-by-orbit basis. These files are provided for quantitative analyses of the CIPS retrievals at high spatial resolution. For those users interested mainly in averaged quantities, the CIPS team also provides level 3C "summary" files – these are files that contain one PMC season each of orbit-by-orbit and daily-averaged quantities binned in 1-degree latitude bins (separate binning for ascending and descending node data). More information can be found in the level 3C documentation.

For an overview of the CIPS measurements and a detailed description of the version 4.20 PMC retrieval algorithm, readers are referred to *Lumpe et al*. [2013; http://dx.doi.org/10.1016/j.jastp.2013.06.007]. The scientific validity of the CIPS v4.20 data was established through its use in a variety of scientific and validation analyses. The v4.20 cloud frequencies and albedo were found to agree very well with coincident measurements from the Solar Back Scatter Ultraviolet (SBUV-2) instruments [Benze *et al*., 2009; 2011]. Baumgarten *et al*. [2012] analyzed CIPS data obtained in close coincidence with ground-based lidar measurements and found good agreement in the cloud brightness observed by these two very different methods. The detailed spatial structures observed by CIPS have been used to study mesospheric gravity waves [Chandran *et al*., 2009; 2010, 2012] and planetary waves [Merkel *et al*. 2009], while the CIPS ice water content has been used by Stevens *et al*. [2010] to analyze the effect of tidal signatures on PMCs. CIPS cloud frequencies were used in Karlsson *et al*. [2011] to connect southern hemisphere (SH) PMC variability with the breakdown of the wintertime SH stratospheric polar vortex. The SH intra-seasonal PMC variability observed by CIPS was also used to investigate inter-hemispheric coupling in Karlsson *et al*. [2009]. Stevens *et al*. [2012] used the CIPS observations of PMC frequency and albedo in July 2011 to help demonstrate a causal link between the occurrence of very bright clouds and the main engine exhaust from the space shuttle's final flight.

This document describes the CIPS PMC v5.20 level 2 data products and provides guidance for data users. The v5.20 PMC dataset is currently being validated by comparison with the CIPS v4.20 data. Results will be summarized and published in a forthcoming paper, which is currently in preparation. Preliminary analyses show the following trends in v5.20 data compared to v4.20: slightly higher cloud frequency, due to increased cloud detection sensitivity; albedos are shifted slightly higher, ~1-2×10^{-6} sr^{-1} on average; particle radius is lower by up to 5 nm on average; ice water content (IWC) is also slightly higher, by ~10-15 g/km^2, consistent with the albedo changes. Based on these initial comparisons we consider the CIPS v5.20 PMC data products to be valid for scientific analysis with the caveats described below.

The publicly available Level 2 data set consists of three NetCDF data files and three png image files for each orbit[1]. Documentation and IDL software tools to read the level 2 NetCDF files are

[1] A fourth file type, with extension _etc.nc, is archived at the NASA Space Physics Data Facility (SPDF). These files contain extra variables that the retrieval development team desired, but that are not part of the publicly distributed data products. For v05.20r05, the variables contained in the file are:
significance_rayleigh: Chi-square significance of the rayleigh parallel component of the residual scattering profile.

available for download from the AIM web site. NetCDF readers for other software packages are available elsewhere (see, for instance, http://www.unidata.ucar.edu/software/netcdf/software.html). These data files are:

(1) Geolocation, including variables such as latitude, longitude, time, etc. The file name extension is _cat.nc.

(2) Cloud properties, including albedo, particle radius, and ice water content. The file name extension is _cld.nc.

(3) Cloud phase function, containing cloud albedo vs. scattering angle. The file name extension is _psf.nc.

(4) Orbit-strip image of cloud albedo. The file name extension is _alb.png.

(5) Orbit-strip image of particle radius. The file name extension is _rad.png.

(6) Orbit-strip image of ice water content. The file name extension is _iwc.png.

The compressed geolocation, cloud property and phase function NetCDF files are ~2, 5, and 13 MB in size, respectively. Uncompressed file sizes are approximately three times larger due to the significant fraction of fill (NaN) values in these files (see below). Most users of level 2 data will not need the cloud phase function file; it is provided mainly for users who wish to re-derive such parameters as cloud particle radius using independent algorithms.

Variables in files (1) through (3) are described in tables at the end of this document. The v05.20 Level 2 data are reported on an equal area Lambert projection grid. Resolution elements are 7.5 km × 7.5 km in the nadir and become elongated away from nadir but remain 56.25 km^2 in total area (this will be rounded to 56 km^2 in the remainder of this document).

There are ~15 orbits per day. Data arrays in the level 2 files provide cloud properties in each 56 km^2 resolution element (hereafter referred to as a level 2 "pixel"), with array dimensions corresponding to the number of elements in the along-track and cross-track directions. Each array element thus corresponds to a unique location (latitude and longitude) that is observed up to ten times with different observation geometries, and thus scattering angles (see *Lumpe et al*. [2013] for a description of the viewing geometry and measurement approach). For convenience in data handling, the arrays span the entire bounding box defined by a CIPS orbit, typically consisting of ~215,000 elements. However roughly half of these elements correspond to locations where no measurements are made and therefore have fill values.

---

significance_nonrayleigh: Chi-square significance of the rayleigh orthogonal subspace of the scattering profile.
sd_n: Noise component of the directional albedo uncertainty.
sd_s: Small scale additional directional albedo uncertainty. This error characterizes the additional average retrieval error in the rayleigh background subtraction after accounting for the noise and the large scale zonal variability in the ozone.
rad_i: Smoothed in fill value for the radius for instances when a good radius cannot be retrieved, but good radius retrievals exist nearby. This is particularly useful for orbit strip edges that have bad scattering angle sampling.
alb_i: Cloud albedo consistent with **rad_i** above. This is used to produce cloud albedo images for which large discontinuities are less common in regions of bad sampling (like orbit strip edges).

The CIPS level 2 PMC retrievals use all Level 1A image data poleward of 30 degrees latitude. All Level 1A pixels at solar zenith angles (SZA) greater than 95 degrees, as well as occasional individual camera images at various SZA, are eliminated to screen out isolated scattered light artifacts that appeared starting in 2012 as the orbit geometry changed. The range of scattering and view angles observed for each location changes along the orbit track. For uniformity and comparison to other data sets, the cloud albedos reported in files (2) and (4) are normalized to 90° scattering angle and nadir (0°) view angle. The view angle correction is accomplished by removing the sec(θ) geometry factor to account for the view angle dependence in path length (where θ, the view angle, is the angle between the satellite and zenith directions, as measured from the scattering volume). The scattering angle correction is accomplished by obtaining the best fit of the observed phase function (albedo vs. scattering angle) to a set of assumed scattering phase functions that are constrained by lidar data (for a comprehensive discussion see Lumpe *et al.* [2013]; also see Hervig *et al*. [2009] and Baumgarten *et al*. [2010]). We make the assumptions that the ice particles have an axial ratio of 2 and a distribution width that varies approximately as 0.39×radius for radii up to 40 nm and then stays fixed at ~ 15.8 nm for larger particles. The albedo at 90° scattering angle from that best fit is the value to which the view angle correction is applied.

From 2007 through 2015 CIPS operated as originally intended, executing a measurement sequence that provided 27 images per orbit in each camera (30 for the PX camera) at a 43-second cadence. Science data images were obtained only in the summer polar regions, covering approximately 8000 km along the orbit and 900 km in the cross-track direction. This operational sequence is known as Summer Pole Imaging. Since February 11, 2016 CIPS has been operating in variations of what is called continuous imaging (CI) mode. In this scenario the image cadence is decreased (typically 2 – 3 minutes) and images are spread out over the entire sunlit portion of the orbit. This change was made in response to the evolution of the AIM orbit, which has precessed from its original midnight (ascending) equator crossing orientation through a terminator (full sun) phase and is now approaching a noon equator crossing (i.e., the satellite is flying backwards relative to its original orientation). The CI modes allow CIPS to make year-round, global measurements of stratospheric gravity waves while still providing PMC measurements in the summer polar region. The trade-off is that the decreased measurement cadence limits the spatial overlap between consecutive images, so that the scattering profiles derived for each Level 2 pixel contain fewer independent measurements compared to the pre-CI mode data (the number of data points in the scattering phase function is denoted by NLAYERS in the Level 2 data files; see Table 1 and the discussion below). Decreasing NLAYERS has implications for the retrieval of particle radius and IWC, as explained below.

2. Orbit Strip Images

Users interested in a quick, qualitative view of the data for a particular orbit should download the albedo image png files, which are type (4) in the list above. In defining the color scale for each image, the plotting routine imposes a limit on the albedo of 2×10^{-6} sr^{-1} as a lower threshold for plotting; thus any clouds dimmer than this will not appear. The upper plotting threshold is set so that 1% of the pixels are saturated, unless this threshold is less than 10^{-5} sr^{-1}, in which case the threshold is set to 10^{-5} sr^{-1}. Since color scales for these png files are determined uniquely for each orbit, these images should not be used to compare cloud brightness from one orbit to the next. For that purpose, users should download the NetCDF files. The particle radius and ice water content images – types (5) and (6) above – are made using the same data screening as is used for the albedo images.

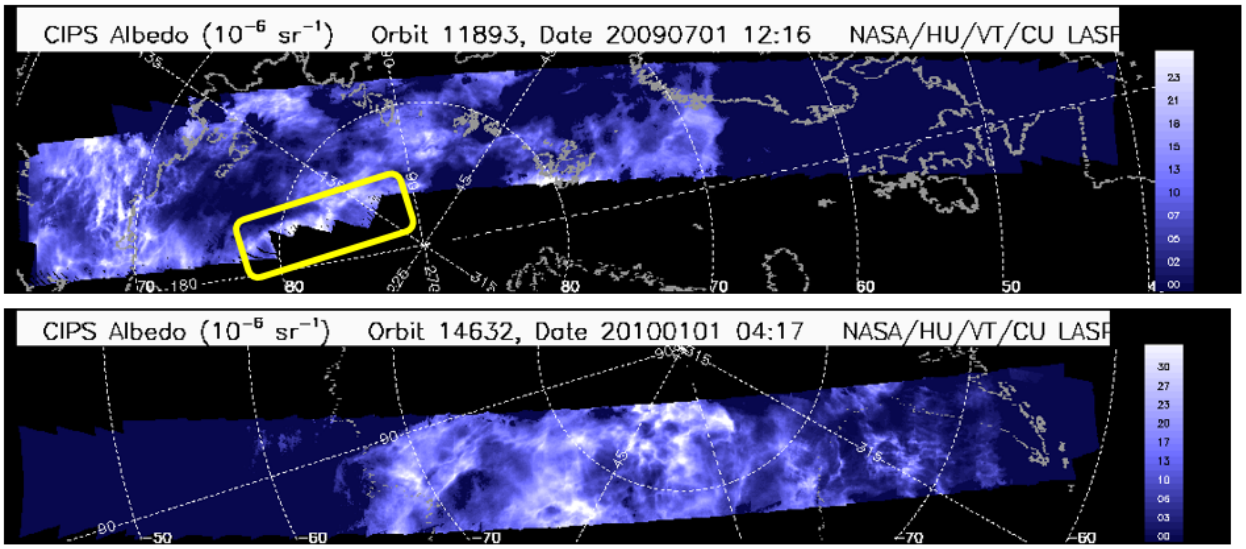

Figure 1. CIPS PMC albedo for orbits 11893 on 1 July 2009 (top) and 14632 on 1 January 2010 (bottom). This sampling is representative of the summer pole imaging sampling from May of 2007 to February of 2015. The discontinuity indicated by the yellow rectangle in the top panel is due to a spacecraft roll, which was required for AIM SOFIE pointing from the NH 2008 PMC season through the SH 2009-2010 season. By 1 January 2010 the effects of the roll on sampling had diminished.

Figure 1 shows examples of Level 2 orbit strip albedo images for both the northern hemisphere (NH, top) and southern hemisphere (SH, bottom) during the Summer Pole imaging mode. These measurements are representative of CIPS observations in the middle of the PMC season from May of 2007 through February of 2016. Latitude lines are drawn in ten-degree increments from 80° to the lowest latitude observed. Each orbit strip nominally consists of overlapping measurements from 27 different 4-camera scenes. As can be seen from these two examples, the CIPS images contain a wealth of information on the cloud structures, which can be analyzed quantitatively using the level 2 NetCDF files.

In March of 2016 CIPS began its Orbit-wide Continuous Imaging mode, in which images were acquired throughout both the day and night sides of the orbit. The night side images cannot be used for PMC retrievals, however. The satellite beta angle, which is the angle between the satellite orbital plane and the vector pointing from the satellite to the sun, changed rapidly from early 2016 through 2018 (approaching -90° in 2017). Because of this, the orientation of the CIPS images varied throughout this time period. Examples of Level 2B orbit strips for 1 July 2016, 1 January 2017, and 1 July 2018 are shown in Figure 2. Early in 2017 AIM entered a “full sun” period, in which the beta angle was between negative 68° and negative 90°, which meant that the spacecraft was in continual sunlight. This necessitated changes in the operations, which previously had relied on the timing of satellite sunrise. Unfortunately, this resulted in an inability to acquire pre-season calibration images for the NH 2017 and SH 2017-2018 seasons, so no PMC data are available for these seasons.

In November of 2018 CIPS began its Sunlit Continuous Imaging mode, in which images were acquired throughout the sunlit side of the orbit, with none taken on the night side. This resulted in

more images being available for PMC retrievals. Examples of the level 2 PMC orbit strips for 1 January 2019, 1 July 2019, 1 January 2020 and 1 July 2020 are shown in Figure 3.

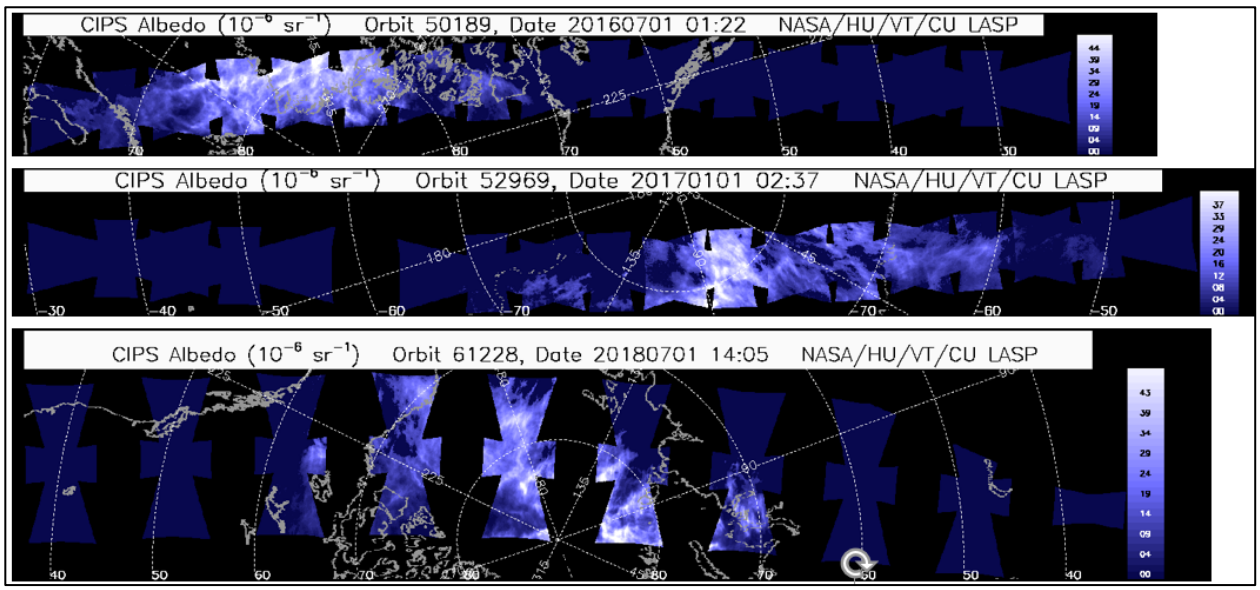

Figure 2. CIPS PMC albedo for orbits 50189 on 1 July 2016 (top), 52969 on 1 January 2017 (middle), and 61228 on 1 July 2018 (bottom). Continuous Imaging operations, where images were acquired throughout the sunlit hemisphere, began in March 2016 and continues to the present. From March 2016 through October 2018, images were acquired on the day and night sides of the orbit, but only dayside images are scientifically useful. This figure illustrates the variable orientation of PMC images as the satellite beta angle changed during this time period. No PMC data are available for the NH 2017 or SH 2017-2018 PMC seasons because of a lack of calibration data.

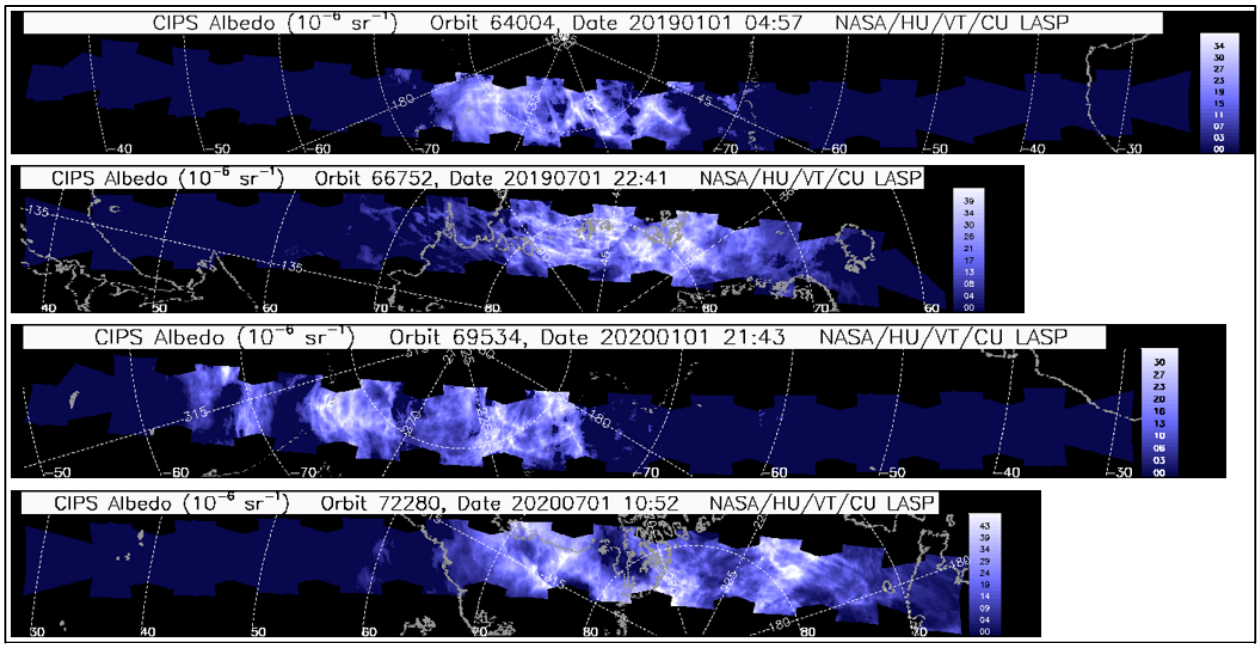

Figure 3. CIPS PMC albedo for orbits 64004 on 1 January 2019, 66752 on 1 July 2019, 69534 on 1 January 2020, and 72280 on 1 July 2020 (top to bottom). From November 2018 to the present, CIPS images are acquired only on the dayside of the orbit, so more scientifically valid images are available on each orbit than during the time period from March 2016 through October 2018.

Sections 2.1 and 2.2 describe two anomalies in the albedo png file images of which users should be aware. If images are found to exhibit suspicious behavior that is not described here, we would very much appreciate being informed (please send an email to aimsds@lasp.colorado.edu).

2.1. Edge Artifacts

On occasion, artifacts near the cross-track edges of the orbits appear like small bits of missing data, an example of which is shown in Figure 4. We are still working to diagnose causes for these artifacts.

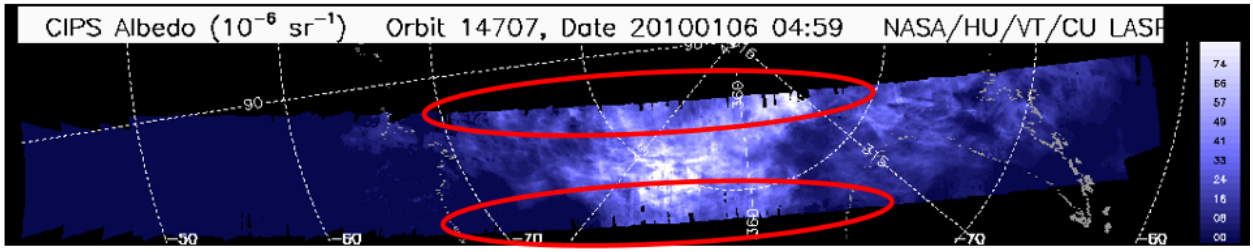

Figure 4. CIPS cloud albedo for orbit 14707 in the SH on 6 January 2010. Black regions inside the red ovals indicate edge artifacts that are not understood at the current time.

2.2. Rolled Images

Beginning in the SH 2007-2008 season and continuing through the SH 2009-2010 season, the AIM satellite rolled to one side during images taken near the common volume (~90° SZA), in order to place the SOFIE line of sight within the CIPS field of view. The amount of roll depended on the satellite beta angle, which changed with time. This led to unusual geometries of the cameras, an example of which was given above in Figure 1, where the change in the orientation of the orbit strip is indicated by the yellow rectangle. The data corresponding to large roll angles can have very high satellite view angles. Because measurements with high view angles are known to have higher than normal systematic errors in the background Rayleigh subtraction, the CIPS retrievals require at least one measurement in the scattering phase function to have a view angle of less than 60°. This criterion gives rise to the zig-zag edge in the orbit strip highlighted by the yellow rectangle in Figure 1; this zig-zag pattern denotes the boundary beyond which view angles are all larger than 60°.

3. Guidance for NetCDF files

The NetCDF files listed in section 1 enable users to quantitatively analyze the data plotted in the orbit strip images. Here we provide guidance for using file types (1) and (2), emphasizing data limitations of which users should be aware. Users interested in the phase function files are encouraged to contact us directly (aimsds@lasp.colorado.edu) for guidance with these files.

3.1. NLAYERS

A critical parameter for evaluating CIPS data quality is NLAYERS, defined as the number of measurements in the scattering phase function in each spatial pixel, from which the cloud albedo, particle radius, and ice water content are derived. As explained above, the CIPS data files report the cloud albedo normalized to 90° scattering angle. This normalization requires information about the scattering phase function, as does the retrieval of cloud particle radius and IWC. When the

scattering phase function is defined by six or more measurements at different scattering angles, the albedo normalization and retrievals of radius and IWC are robust. Larger uncertainties are inherent in retrievals with measurements at fewer scattering angles, and particle radius and ice water content are not reported for NLAYERS < 2. And because of the normalization uncertainty, caution is warranted when interpreting albedo values for pixels with NLAYERS < 2.

In the summer pole imaging mode (prior to late February 2016), most geographic locations viewed by CIPS were measured in more than 5 successive scenes, with different scattering angles each time. Locations at the cross-track edges of the orbits, however, correspond to lower values of NLAYERS, so retrievals at the cross-track edges in summer pole imaging mode will have higher uncertainties. As discussed above, in continuous imaging mode, which began in late February 2016, there is significantly less overlap between successive images, resulting in lower NLAYERS values everywhere in the orbit. Specifically, there are no Level 2 pixels with NLAYERS > 3 in this imaging mode, so users will find many fewer radius and IWC retrievals in the continuous imaging mode data.

3.2. Solar Zenith Angle Screening

The CIPS measurement sampling is a function of solar zenith angle (SZA) along the orbit path. This sampling is a primary determinant of our ability to adequately define the scattering phase function. Ideally, the measurements of a single location would include six or more observations, covering a wide range of scattering angles. The geometry of the CIPS observations dictates, however, that the range of scattering angles sampled at any given SZA decreases with decreasing SZA (see Figure 5). At high SZA, CIPS samples more forward scattering (scattering angles less than 90°). For typical PMC particle sizes, forward scattering is stronger than backward scattering, so signals are largest at small scattering angles, all other things being equal. This, combined with the fact that background Rayleigh scattering decreases at high SZA, enhances the discrimination between cloud and background contributions in the measured scattering phase function, and hence increases the detection sensitivity at high SZA. The CIPS cloud detection sensitivity improves as more forward scattering angles are sampled in the scattering profile. CIPS is therefore more

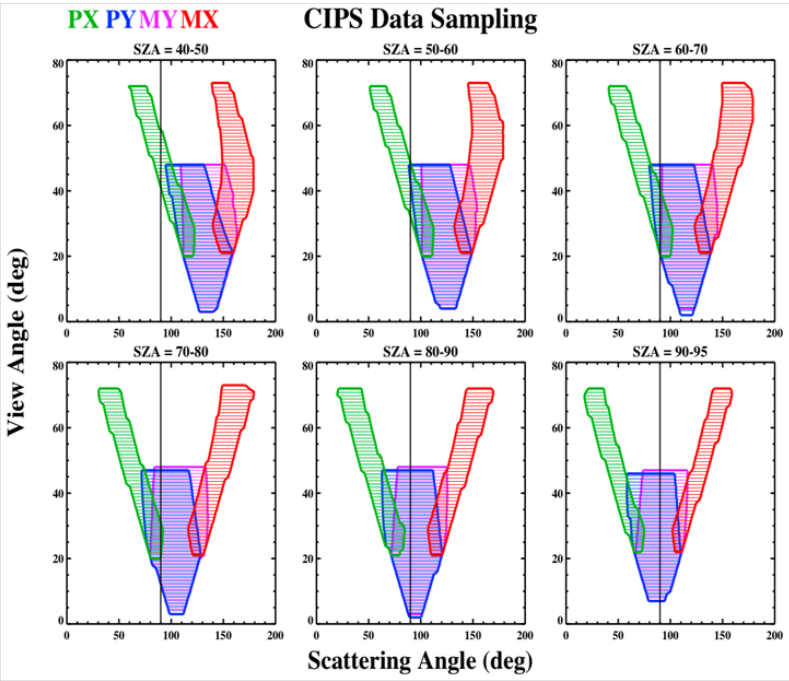

Figure 5. This figure illustrates the typical range of view angle and scattering angle sampled by each CIPS camera, and their dependence on solar zenith angle. Each panel corresponds to a different solar zenith angle bin, ranging from 40 to 95 degrees. This sampling pattern is the same in both hemispheres. From Lumpe *et al.* [2013].

sensitivity to dim clouds at higher SZA, and the minimum detectable cloud brightness increases as the SZA decreases.

3.4. Albedo Threshold

The accuracy with which a cloud is detected, and with which the properties of albedo, particle size, and IWC are determined, naturally depends on the cloud albedo, since this dictates the amount of light scattered to the detector. Figure 6 compares cloud parameters that are obtained for the NH 2010 season when averaging over only those measurements for which the albedo is larger than 3×10^{-6} sr^{-1} (left), 6×10^{-6} sr^{-1} (middle), or 10×10^{-6} sr^{-1} (right). Defining a standard CIPS albedo unit as 1 "G" = 10^{-6} sr^{-1}, these thresholds are equivalent to 3G, 6G, and 10G. The advantage of using lower thresholds is that more (total) clouds are detected. The advantage of using higher thresholds is that fewer false detections are included. The plots in Figure 6 were made with the level 3C

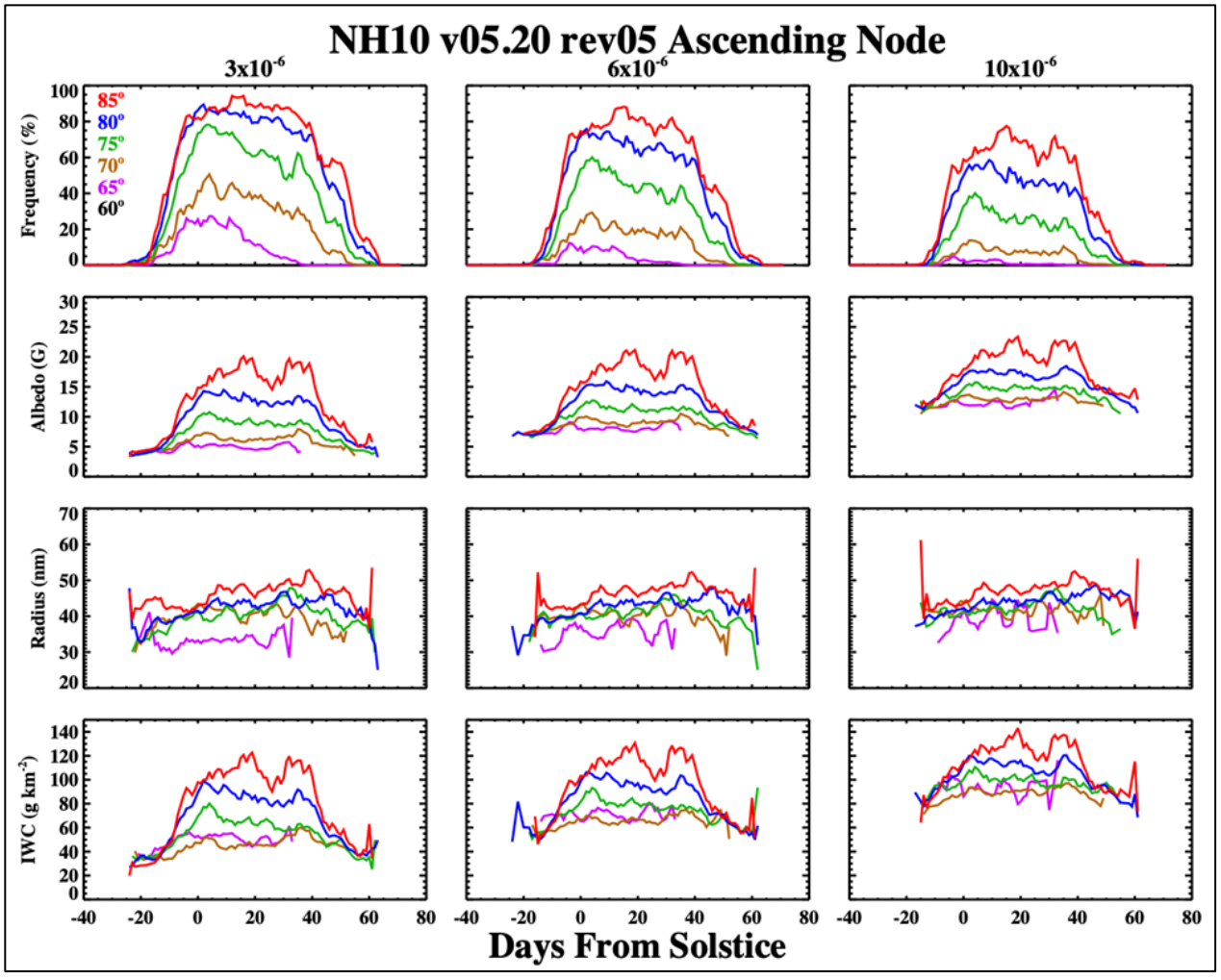

Figure 6. CIPS ascending node PMC frequencies (top), albedo (row 2), radius (row 3), and IWC (bottom) for the NH 2010 season. The columns show the results for measurements that include only those clouds brighter than 3×10^{-6} sr^{-1} (left), 6×10^{-6} sr^{-1} (middle) and 10×10^{-6} sr^{-1} (right). Colors correspond to latitude, as denoted by the labels in the top left panel. The plots were made with level 3C data.

"summary" files, for which the data were binned into 1-degree latitude bins (see the level 3C documentation). In addition, level 3C data omit all measurements with SZA>94° and with radius ≤ 20 nm. Recall also that if NLAYERS < 3, no radius or IWC data are reported in the level 2 files, so by definition the level 3C files will also not contain these data. The Figure 6 plots of albedo, radius, and IWC show values only for cloud points (cloud_presence_map = 1; see Table 2 below); they do not average in non-cloud data. Data were binned separately for the ascending and descending nodes, and Figure 6 presents results for the ascending node. Descending node results are qualitatively similar, except as discussed below.

As expected, cloud frequencies shown in Figure 6 are somewhat higher for the 3G threshold than for the 6G or 10G thresholds. False detection rates will also be higher with lower thresholds compared to higher thresholds. However, the false detection rate in CIPS v05.20 PMC data, which can be empirically determined by looking at the observed cloud "detections" outside of the known PMC cloud season, are extremely low, on the order of 10^{-3} %. CIPS v5.20r05 derived frequencies are generally valid for scientific analysis for clouds with albedo ≥ 5×10^{-6} sr^{-1}.

Figure 6 shows that the general morphology for frequency, albedo, and IWC is similar for all thresholds, with largest values at the highest latitudes and in the middle of the season. Note that removal of the dimmest clouds in the 6G and 10G plots results in missing data around the edges of the distributions (early or late in the season, and at the low-latitude edge). The average albedo increases with increasing threshold, since the dimmer clouds are not included in the average for the higher thresholds. Correspondingly, the average IWC also increases.

3.5. Summary

Although the CIPS data are available with minimal screening, we recommend that users apply certain screening themselves when analyzing the data, as summarized here.

NLAYERS: We consider the CIPS albedo data to be robust for values of NLAYERS ≥ 2. While albedo is reported for NLAYERS = 1 pixels these retrievals may be biased due to the fact that a default particle size must be assumed to translate the directional albedo at the measured scattering angle to the 90° albedo reported in the CIPS Level 2 data files. For quantitative interpretations of radius and IWC, best results will be obtained for pixels with NLAYERS ≥ 3. We do not provide radius or IWC values if NLAYERS < 2.

Albedo Threshold: For qualitative purposes, such as investigations of cloud presence and large-scale patterns, we recommend that only data with albedo larger than 5×10^{-6} sr^{-1} (5G) be used. Note that this is a conservative threshold, and often the retrievals are robust even when the albedo is as low as 3×10^{-6} sr^{-1}, as shown in Figure 6.

Radius: Only data with radius > 20 nm should be used for scientific analyses.

Additional notes and caveats:

Each NetCDF file of type (1) – (3) has a day-of-year included in the file name. This is the day corresponding to the ascending node equator crossing time. When the equator crossing time is near midnight UT, some or all of the data in the file occur on the day after the day in the filename.

Users should be aware that in some of the data files, there is an error in the parameter Orbit_Start_Time_UT. When the error occurs, the symptom is that the yyyymmdd part of Orbit_Start_Time_UT refers to the day the orbit strip finished, rather than the day it started. The error only occurs when the orbit crosses midnight UT, and only on some of these orbits. Whether the error occurs depends on the time between the midnight crossing and start of data collection, so it occurs much more often in the SH than in the NH. No PMC data are affected by this error; it is only in the Orbit_Start_Time_UT variable.

Table 1. Variables in the CIPS level 2 geolocation ("cat") file. Fill value is NaN.

Variable Name	Units	Type/Dimension	Description
AIM_Orbit_Number		Integer / 1	Integer orbit number to which all data in the file applies
Version		String / 1	Data version number
Revision		String / 1	Data revision number
Product_Creation_Time		String / 1	String containing UT time at which data file was produced
UT_Date		Long / 1	UT date in yyyymmdd format
Hemisphere		String / 1	N (north) or S (south)
Orbit_Start_Time	microseconds	Double / 1	GPS start time of orbit (microseconds from 0000 UT on 6 Jan 1980)
Orbit_Start_Time_UT	seconds	String / 1	Start time of orbit in yyyy/doy-hr:min:sec format
Orbit_End_Time	microseconds	Double / 1	GPS end time of orbit (microseconds from 0000 UT on 6 Jan 1980)
Stack_ID		Integer / 1	Obsolete.
XDim		Long / 1	Number of along-orbit-track elements in the data arrays
YDim		Long / 1	Number of cross-orbit-track elements in the data arrays
UT_Time	hours	Float / [xdim,ydim]	UT time for each element (fractional hour)
NLayers		Integer / [xdim,ydim]	Number of observations at the location of each element; each observation corresponds to a different observing geometry and thus scattering angle in the phase function
Quality_Flags		Float / [xdim,ydim]	Indicators of data quality for each element. QF=0 indicates valid data. QF=2 indicates the cloud layer is completely in shadow (solar zenith angle > 94 deg.
KM_Per_Pixel	km	Float / 1	Linear dimension of square pixel occupying area of CIPS resolution element
BBox	Index	Long / [4]	Bounding Box: Bottom-Left and Top-Right indices of the smallest rectangle which both circumscribes a set of cells on a grid and is parallel to the grid axes

Center_Lon	Degrees	Double / 1	Center longitude of the orbit
Latitude	Degrees	Float / [xdim,ydim]	Latitude of each element; Latitudes greater (less) than 90 (-90) indicate ascending node data.
Longitude	Degrees	Float / [xdim,ydim]	Longitude of each element; ranges from -180 to 180
Zenith_Angle_Ray_Peak	Degrees	Float / [xdim,ydim]	Solar zenith angle (SZA) of each element. The value is specified at the altitude of the maximum contribution to the Rayleigh background. Generally around 55 km but increasing with increasing SZA.
Common_Volume_Map		Byte / [xdim,ydim]	Indicator for whether this location is within the single "Common Volume" where both CIPS and SOFIE observe each orbit. Indicator 1 = in the common volume; 0 = not in the common volume.
Notes		String	Any additional notes

Table 2. Variables in the CIPS level 2 cloud parameters ("cld") file. Fill value is NaN.

Variable Name	Units	Type/Dimension	Description / Example*
Percent_Clouds	Percent	Float / 1	Ratio (×100) of the # clouds detected (cloud_presence_map = 1) to the # locations where it was possible to detect a cloud (cld_albedo ≥ 1).
Significance_Threshold	N/A	Float / 1	Chi-square significance threshold.
Significance	N/A	Float / [xdim,ydim]	Estimated odds that the measurement and retrieval errors would cause this level of significance. Significance above the significance threshold are flagged as cloud detections in the cloud presence map.
Cloud_albedo_sensitivity	10^{-6} sr^{-1}	Float / [xdim,ydim,4]	Cloud albedo required to meet the significance threshold for each mode radius on the "cloud albedo sensitivity radius grid". A real cloud at this albedo may or may not reach the significance threshold depending on the particular measurement/retrieval errors.

Cloud_albedo_sensitivity_radius_grid	nm	Float / 4	Radius grid for the cloud albedo sensitivity.
Albedo_to_iwc_sensitivity_convert	(µg m^{-2}) / (10^{-6} sr^{-1})	Float / 4	Conversion factor to convert the cloud albedo sensitivity into an IWC sensitivity. There is one factor for each radius on the grid.
Cloud_Presence_Map		Float / [xdim,ydim]	Indicator for whether a cloud was detected (1) or not (0).
Cld_Albedo	10^{-6} sr^{-1}	Float / [xdim,ydim]	Residual PMC albedo, defined as the albedo, after subtracting the Rayleigh background, that would be viewed at 90° scattering angle and 0° view angle. (Note – this array is populated for both cloud and non-cloud pixels, and negative values are possible).
Cld_Albedo_Unc	10^{-6} sr^{-1}	Float / [xdim,ydim]	Cloud albedo uncertainty.
Particle_Radius	nm	Float / [xdim,ydim]	Retrieved particle mode radius, defined as the mean radius for a Gaussian distribution of particles with an axial ratio of 2 and a distribution width that varies as 0.5×radius. Zero means no cloud was detected. A value of -999 is reported if QF>1.
Particle_Radius_Unc	nm	Float / [xdim,ydim]	Particle radius uncertainty.
Ice_Water_Content	µg m^{-2}	Float / [xdim,ydim]	Ice water content at each observation location. Zero means no cloud was detected. A value of -999 is reported if QF>1.
Ice_Water_Content_Unc	µg m^{-2}	Float / [xdim,ydim]	Ice Water Content uncertainty.
Ice_Column_Density	ice particles cm^{-2}	Float / [xdim,ydim]	Ice Column Density. Zero means no cloud was detected. A value of -999 is reported if QF>1..
Ice_Water_Content_Air	µg m^{-2}	Float / [xdim,ydim]	Alternative ice water content derived from the Albedo Ice Regression (AIR) method.
Ice_Water_Content_Air_Unc	µg m^{-2}	Float / [xdim,ydim]	AIR ice Water Content uncertainty.

Cld_Albedo_Air	10^{-6} sr^{-1}	Float / [xdim,ydim]	Alternative PMC albedo derived from the Albedo Ice Regression (AIR) method.
Cld_Albedo_Air_Unc	10^{-6} sr^{-1}	Float / [xdim,ydim]	AIR cloud albedo uncertainty.

Table 3. Variables in the CIPS level 2 phase function file. Fill value is NaN.

Variable Name	Units	Type/Dimension	Description / Example*
Cld_Phase_Albedo	10^{-6} sr^{-1}	Float / [xdim,ydim,nlayers]	Cloud scattering phase function - albedo vs. scattering angle. The number of data points in each pixel is given by the Nlayers array (see Table 1; holds for all arrays in this file). / [1164,187,10], range: -15.24 to 633.70.
Cld_Phase_Albedo_Unc	10^{-6} sr^{-1}	Float / [xdim,ydim,nlayers]	Uncertainty in cloud phase function. [1164,187,10],
Scattering_Angle	Degrees	Float / [xdim,ydim,nlayers]	Scattering angle for each measured data point. / [1164,187,10], range: 20.69 to 179.96.
View_Angle_Ray_Peak	Degrees	Float / [xdim,ydim,nlayers]	Satellite view angle for each measured data point. /[1164,187,10], range: 0.32 to 72.29.

References

Baumgarten, G., A. Chandran, J. Fiedler, P. Hoffman, N. Kaifler, J. Lumpe, A. Merkel, C. E. Randall, D. Rusch, and G. Thomas, On the horizontal and temporal structure of noctilucent clouds as observed by satellite and lidar at ALOMAR (69N), *Geophys. Res. Lett.*, 39, L01803, doi:10.1029/2011GL049935, 2012.

Baumgarten, G., J. Fiedler, and M. Rapp, On microphysical processes of noctilucent clouds (NLC): observations and modeling of mean and width of the particle size distribution, Atmos. Chem. Phys. 10, 6661-6668, doi:10.5194/acp-10-6661-2010, 2010.

Benze, S., et al., Comparison of polar mesospheric cloud measurements from the Cloud Imaging and Particle Size experiment and the solar backscatter ultraviolet instrument in 2007, JASTP 71, 365-372, doi:10.1016/j.jastp.2008.07.014, 2009.

Benze, S., et al., Evaluation of AIM CIPS measurements of Polar Mesospheric Clouds by comparison with SBUV data. Journal of Atmospheric and Solar-Terrestrial Physics, doi:10.1016/j.jastp.2011.02.003, 2011.

Chandran, A., D.W. Rusch, G.E. Thomas, S.E. Palo, G. Baumgarten, E.J. Jensen, and A.W. Merkel, Atmospheric gravity wave effects on polar mesospheric clouds: A comparison of numerical simulations from CARMA 2D with AIM observations, *J. Geophys. Res.*, doi:10/1029/2012JD017794, 2012.

Chandran, A., D. W. Rusch, A. W. Merkel, S. E. Palo, G. E. Thomas, M. J. Taylor, S. M. Bailey, and J. M. Russell III, Polar Mesospheric Cloud structures observed from the CIPS experiment on the AIM spacecraft: Atmospheric gravity waves as drivers for longitudinal variability in PMC occurrence, *J. Geophys. Res.*, doi:10.1029/2009JD013185, 2010.

Chandran, A., D. W. Rusch, S. E. Palo, G. E. Thomas, and M. Taylor, Gravity wave observation from the Cloud Imaging and Particle Size (CIPS) Experiment on the AIM Spacecraft, *J. Atmos. Solar-Terr. Phys*., doi:10.1016/j.jastp.2008.09.041, 2009.

Hervig, M.E., et al., Interpretation of SOFIE PMC measurements: Cloud identification and derivation of mass density, particle shape, and particle size, JASTP 71, 316-330, doi:10.1016/j.jastp.2008.07.009, 2009.

Karlsson, B. M., C. E. Randall, T. G. Shepherd, V. L. L. Harvey, J. D. Lumpe, K. Nielsen, S. M. Bailey, M. E. Hervig, and J. M. Russell III, On the seasonal onset of polar mesospheric clouds and the breakdown of the stratospheric polar vortex in the southern hemisphere (2011), *J. Geophys. Res.*, 116, D18107, doi:10.1029/2011JD015989, 2011.

Karlsson, B., C.E. Randall, S. Benze, M. Mills, V.L. Harvey, S.M. Bailey, J.M. Russell III, Intraseasonal variability of polar mesospheric clouds due to inter-hemispheric coupling, *Geophys. Res. Lett*., VOL. 36, L20802, doi:10.1029/2009GL040348, 2009.

Lumpe, J. D., S.M. Bailey, J.N. Carstens, C.E. Randall, D. Rusch, G.E. Thomas, K. Nielsen, C. Jeppesen, W.E. McClintock, A.W. Merkel, L. Riesberg, B. Templeman, G. Baumgarten, and J.M. Russell, III, Retrieval of polar mesospheric cloud properties from CIPS: algorithm description, error analysis and cloud detection sensitivity, *J. Atmos. Solar-Terr. Phys.*, http://dx.doi.org/10.1016/j.jastp.2013.06.007, 2013.

Merkel, A. W., D. W. Rusch, S. E. Palo, J. M. Russell III, and S. M. Bailey, Mesospheric planetary wave activity inferred from AIM-CIPS and TIMED-SABER for the northern summer 2007 PMC season. *J. Atmos. Solar-Terr. Phys.*,doi:10.1016/j.jastp.2006.05.01, 2009.

Stevens, M. H., S. Lossow, J. Fiedler, G. Baumgarten, F.J. Lübken, K. Hallgren, P. Hartogh, C.E. Randall, J. Lumpe, S.M. Bailey, R. Niciejewski, R.R. Meier, J.M.C. Plane, A.J. Kochenash, D.P. Murtagh, C.R. Englert, Bright polar mesospheric clouds formed by main engine exhaust from the space shuttle's final launch, *J. Geophys. Res.*, 117, D19206, doi:10.1029/2012JD017638, 2012.

Stevens, M. H., D. E. Siskind, S. D. Eckermann, L. Coy, J. P. McCormack, C. R. Englert, K. W. Hoppel, K. Nielsen, A. J. Kochenash, M. E. Hervig, C. E. Randall, J. Lumpe, S. M. Bailey, M. Rapp & P. Hoffmann, Tidally induced variations of polar mesospheric cloud altitudes and ice

water content using a data assimilation system, *J. Geophys. Res.*, 115, D18209, doi:10.1029/2009D013225, 2010.

Created by Jerry Lumpe and Cora Randall, August 2020